A FINITE ELEMENT INVERSE ANALYSIS TO ASSESS FUNCTIONAL IMPROVEMENT DURING THE FRACTURE HEALING PROCESS

By

Jared Anthony Weis

Thesis

Submitted to the Faculty of the

Graduate School of Vanderbilt University

in partial fulfillment of the requirements

for the degree of

MASTER OF SCIENCE

in

Biomedical Engineering

December, 2009

Nashville, Tennessee

Approved:

Professor Michael I. Miga

Professor Robert J. Roselli

TABLE OF CONTENTS

LIST OF TABLES

Table Page

LIST OF FIGURES

ACKNOWLEDGMENTS

This work was supported by a National Institutes of Health Grant 5R01DK070929-02 (to Dr. Anna Spagnoli). I also acknowledge the technical support of the Vanderbilt Institute of Imaging Science at Vanderbilt University and the Biomedical Research Imaging Center at University of North Carolina at Chapel Hill.

CHAPTER I

INTRODUCTION

Approximately 10-20% of the 6.2 million annual bone fractures result in fracture healing failure (non-union), causing significant morbidity and mortality (Einhorn, 1995; Marsh, 1998). In long-bones, fracture healing proceeds through the formation of a cartilaginous template that is then replaced by bone that undergoes remodeling (Einhorn, 1998). Fracture healing is a postnatal repair process that recapitulates aspects of the embryonic development of the skeleton. It proceeds via callus formation and an endochondral ossification sequence, where cartilage forms, matures, undergoes hypertrophy, and is eventually replaced by the new bone that bridges the fracture gap. The newly formed cartilage stabilizes the fracture and provides a template for new bone formation. (Hall and Miyake, 1992; Roark and Greer, 1994; Hall and Miyake, 1995; Ganan et al., 1996; Chen and Zhao, 1998; Macias et al., 1999; Hall and Miyake, 2000; Capdevila and Izpisua Belmonte, 2001; Mariani and Martin, 2003).

A critically important function of bone healing is that the healing tissue provides sufficient mechanical stabilization such that a return to functionality is possible. Because fracture healing is a phenomenon that modulates the mechanical stability of a broken bone, there is an important clinical need to monitor the mechanical properties of a healing callus so that a clinician may detect and intervene in the event of non-union. Also, many fracture healing rodent models within the context of experimenting novel treatments for enhancing the fracture repair process have been developed (Holzer et al., 1999;

Huddleston et al., 2000; Zhao et al., 2005; Granero-Molto et al., 2007; Zachos et al., 2007; Granero-Molto et al., 2008; Gutierrez et al., 2008). To determine the efficacy of these treatments, there is an important need to monitor and characterize the load-bearing mechanical properties within the context of the experimental fracture callus system. However, the lack of sensitive methods to monitor and relate the fracture mechanical properties with tissue type renders those studies inadequate to fully evaluate the fracture healing patho-physiology. Therefore, the goal of this research was to develop a finite element modeling (FEM) approach, combining micro-computed tomography and biomechanical testing to use in evaluating mechanical properties as a biomarker in the assessment of fracture healing progression. This approach relies on the use of an elastographic inverse FEM framework that uses traditional forward FEM techniques iteratively to make estimations of the callus tissue elastic modulus.

CHAPTER II

A FINITE ELEMENT INVERSE ANALYSIS TO ASSESS FUNCTIONAL IMPROVEMENT DURING THE FRACTURE HEALING PROCESS

Abstract

Assessment of the restoration of load-bearing function is the central goal in the study of fracture healing process. During the fracture healing, two critical aspects affect its analysis: (1) material properties of the callus components, and (2) the spatio-temporal architecture of the callus with respect to cartilage and new bone formation. In this study, an inverse problem methodology is used which takes into account both features and yields material property estimates that can analyze the healing changes. Six stabilized fractured mouse tibias are obtained at two time points during the most active phase of the healing process, respectively 10 days (n=3), and 14 days (n=3) after fracture. Under the same displacement conditions, the inverse procedure estimations of the callus material properties are generated and compared to other fracture healing metrics. The FEA estimated property is the only metric shown to be statistically significant ($p=0.0194$) in detecting the changes in the stiffness that occur during the healing time points. In addition, simulation studies regarding sensitivity to initial guess and noise are presented; as well as the influence of callus architecture on the FEA estimated material property metric. The finite element model inverse analysis developed can be used to determine the effects of genetics or therapeutic manipulations on fracture healing in rodents.

Introduction

Bone fracture healing is a complex biological process, and assessment of fracture healing has relied on histological, imaging, and biomechanical testing (BMT) (Gerstenfeld et al., 2005). Histological methods allow the visualization of tissue-specific molecules over histological sections by in-situ hybridization, immunohistochemistry, or specific staining. However, comparisons between sections are difficult and true quantitative assessment is unrealistic. Furthermore, histological methods are limited to *post-mortem* analysis and cannot provide functional information. Various imaging modalities have been used to assess the fracture healing, such as micro-computed tomography (μCT), magnetic resonance, and positron emission tomography (Cattermole et al., 1996; Grigoryan et al., 2003; Ciprian et al., 2004; Lynch et al., 2004; Severns et al., 2004; Schmidhammer et al., 2006; Hsu et al., 2007; Saran and Hamdy, 2008). μCT imaging is mostly used due to advantages in 3D reconstructions. However, imaging provides no information about tissue types and mechanical properties. BMT remains the gold standard for the functional assessment of fracture healing. Standard BMT analyses use force versus displacement data and analytic calculations based on beam theory to generate mechanical property information. Beam theory calculations rely on the assumption of a homogeneous cross section, but because of the irregular geometry of the callus, these calculations are strongly biased by geometrical factors (van Lenthe et al., 2008).

Some studies have explored coupling μCT imaging with finite element analysis (FEA) to predict the mechanical behavior based on geometrical information. In particular, studies have evaluated μCT attenuation to stiffness value transformations to

provide material properties and found empirical power law relationships between modulus and bone mineral content assessed by μCT attenuation/density (Bourne and van der Meulen, 2004; Shefelbine et al., 2005). Shefelbine and colleagues have also reported a weak correlation between predicted and experimental torsional rigidity with a very poor predictive value in calluses studied at early healing stages when mineralization is low (Bourne and van der Meulen, 2004; Shefelbine et al., 2005). It is quite apparent that the direct relationship between μCT attenuation/density and mechanical parameters is unclear and is to some degree unsatisfactory; and when factoring in the potential for variability of this relationship across experimental systems, it is unlikely that the correlation will improve.

In our studies, rather than using a μCT-to-stiffness empirical relationship, we have used an elastographic approach to directly generate values for mechanical parameters. Our approach combines an inverse finite element model of the subject's cartilage/bone geometry (μCT/histological imaging data), data acquired from BMT, and numerical optimization techniques to characterize the callus mechanical properties. This approach does not require calibration in each system but rather is an active reconstruction parameter that can be measured experimentally. The concept of an 'inverse' FE analysis method to determine the mechanical parameters to monitor the progression of fibrogenic diseases has been demonstrated. These techniques are more widely referred to as elastography (Ophir et al., 1991; Greenleaf et al., 2003; Washington and Miga, 2004; Miga et al., 2005; Barnes et al., 2007; Samani and Plewes, 2007; Ou et al., 2008). Within this work, the approach is used to evaluate mechanical properties as a biomarker in the assessment of fracture healing progression. Quantifying the change in mechanical

properties during the fracture healing process may provide information that: (1) allows to determine when healing has failed to progress, (2) suggests the need for intervention in non-union/slow healing fractures, and (3) evaluates the effectiveness of treatments that aim to enhance the healing process through the formation of more mechanically competent tissue.

Methods

Generation of the Computational Model

An inverse FEA procedure was developed to determine the stiffness of the callus based on μCT imaging and BMT data. As summarized in Figure 1, the procedure begins with the establishment of an assumed Hookean linear elastic tissue model framework for the bone/callus system. The process continues with the development of a bone/callus computer model of the subject generated from μCT image volumes. A volumetric tetrahedral grid is then generated to represent a FE mesh system.

The boundary conditions for the model were chosen to reflect the BMT protocol, in which the top boundary is prescribed a fixed upward normal displacement with no lateral displacement (Dirichlet boundary conditions). The bottom surface was also fixed in both the normal and lateral direction. The remaining boundary conditions for the sides of the model were stress free. The displacement criteria selected for each sample was based on the individual force/displacement curve obtained from BMT. A series of four displacements were taken along the curve at 25%, 50%, 75%, and 100% of the linear

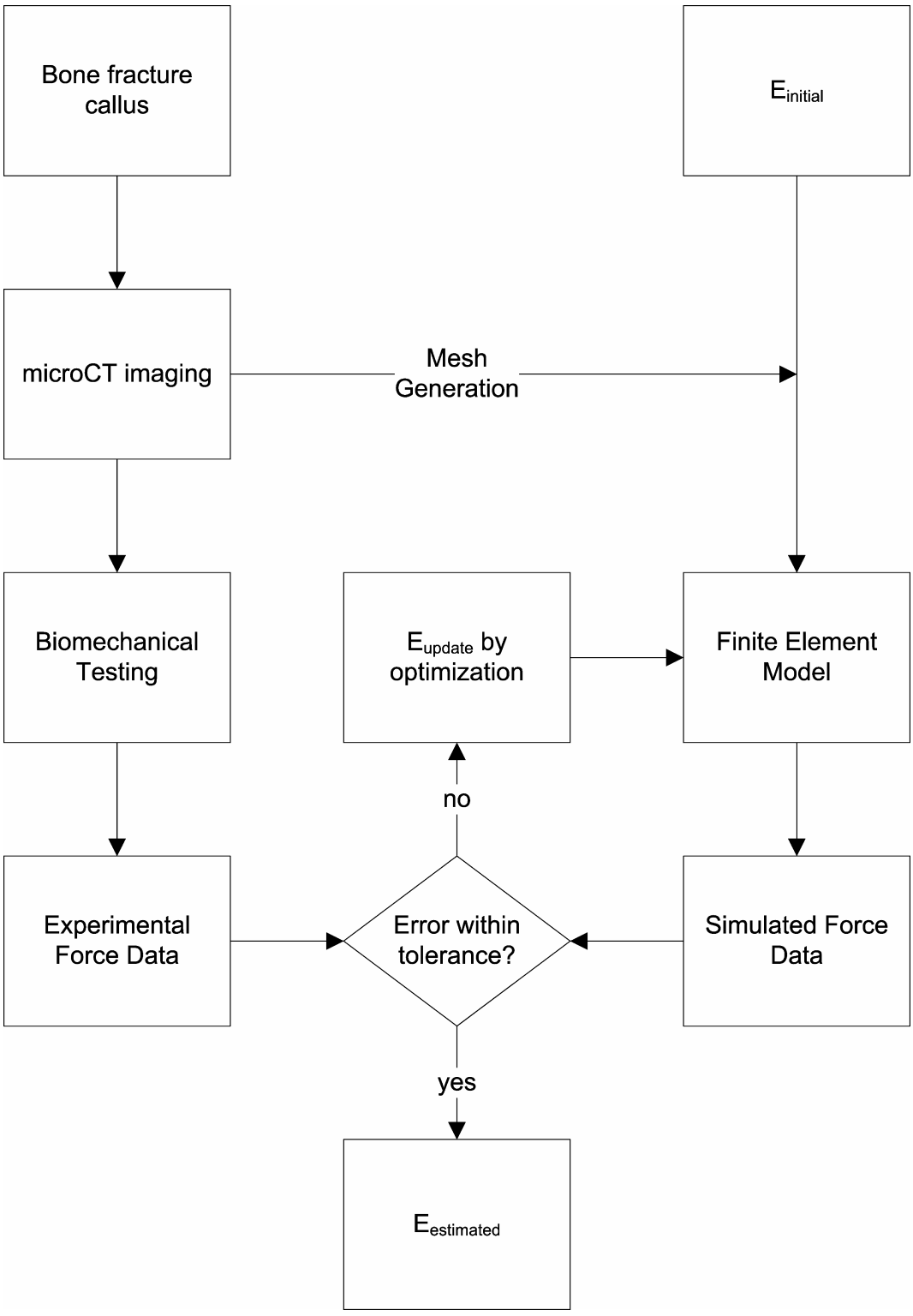

Figure 1: General framework of the inverse material property reconstruction method. The stiffness is iteratively reconstructed by comparing model calculated forces to biomechanical testing forces.

elastic limit to reproduce the linear portion of the curve. As pointed out in Figure 2, the linear elastic limit was defined as the point at which the curve exhibited plastic deformation (slope ≤ 0 in our case). Solutions to the elastic system are then generated as reported previously (Barnes et al., 2007). As shown by Barnes and colleagues, the unused Galerkin equations associated with the implementation of the Dirichlet boundary conditions are utilized post model-execution to estimate the local boundary stress (Barnes et al., 2007). This stress is then averaged over the tensile boundary surface and multiplied by the surface area to generate a model-calculated average force (F_{calc}) applied to the bone surface for the given displacement. The model is solved at each displacement value to generate four model-calculated average forces which are compared to the corresponding forces measured from the force/displacement curve in a least squares sense and properties of the callus determined through an iterative optimization process. A further discussion of the inverse problem framework is discussed in Appendix B.

Experimental model

Mouse Stabilized Tibia Fracture Model

Female FVB-NJ mice (Jackson Laboratories) 8-12 weeks old were anesthetized using isofluorane to provide deep anesthesia. Pin stabilized mid-diaphyseal tibia fractures were generated by insertion of a 0.25 mm stainless steel pin (Fine-Science-Tools) through the tibial tuberosity followed by fracture creation using a three-point bending device with a standardized force (Einhorn, 1995). Immediately following tibia fracture, 0.5 mg/kg of bupremorphine was administered for pain control. On post-

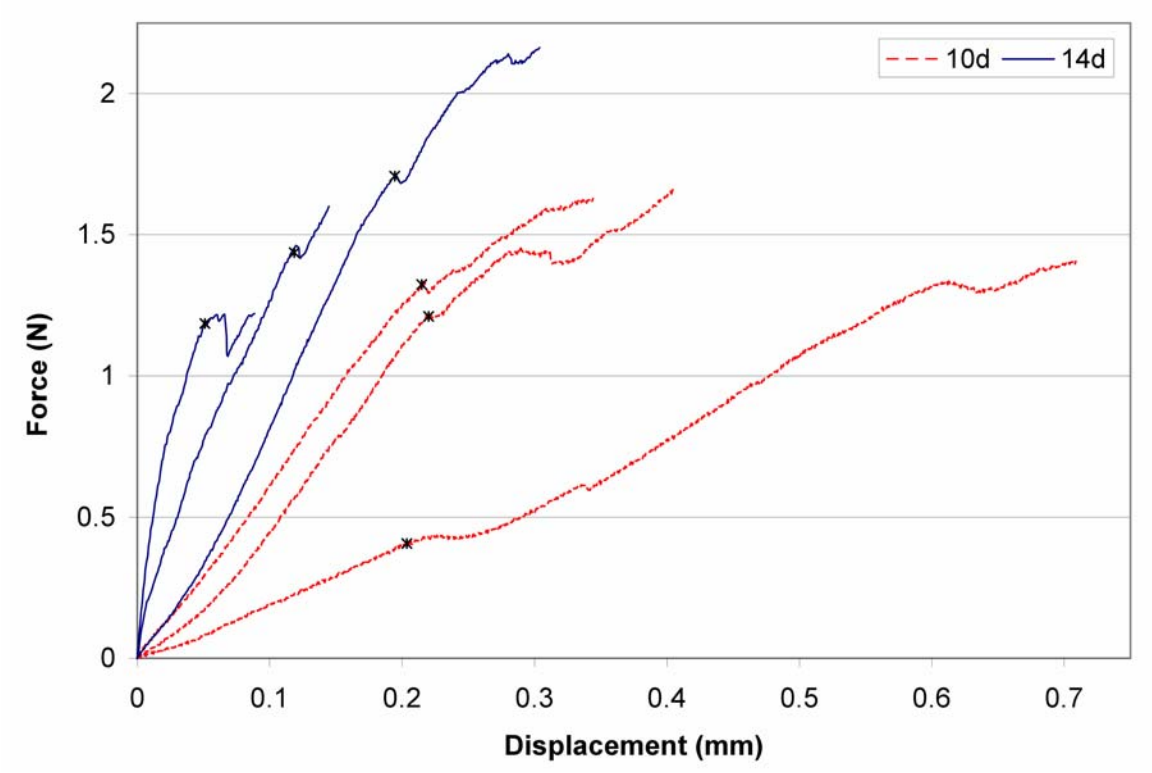

Figure 2: BMT force versus displacement data of each tibia fracture callus tested at day 10 and day 14 post fracture during tensile testing. Note the wide sample variation within each group, demonstrating confounding geometrical effects. Asterisk denotes linear elastic limit.

fracture days 10 and 14, mice were euthanized, fractured tibias were dissected and wrapped in phosphate buffered saline soaked gauze and stored at -80 °C until further analysis. Animal studies were approved by the Institutional Animal Care and Use Committee at Vanderbilt University Medical Center and the University of North Carolina at Chapel Hill.

Callus μCT IImaging and μCT/Histological Thresholding Analyses

μCT scans were performed using a Scanco μCT 40 scanner (Scanco Medical) and were obtained at 55 kVp, 145 μA, 300 ms integration time using 12 μm voxel resolution along 5.2 mm length centered at the fracture line (Reynolds et al., 2007). μCT reconstructions were used for subsequent FEA and volume measurements. To determine material type (newly mineralized bone, highly mineralized bone and cartilage) and quantify callus volumes from μCT scans, a parametric thresholding study was performed by serial μCT scanning and histological analysis as more extensively reported within Appendix B.

BMT Analyses

Fractured tibia ends were embedded into a polymethylmethacrylate cast using custom designed testing fixtures, leaving the fracture callus exposed. Specimens were kept fully hydrated with PBS during the entire testing procedure. The fixtures were loaded into an Enduratec Electroforce 3100 mechanical tester (Bose, Enduratec Systems Group) and tested in tension at a fixed displacement rate of 0.25 mm/min using a 22 N transducer (Honeywell Sensotec) for force data (Colnot et al., 2003). Displacement and

force were recorded until failure and used for subsequent FEA and to determine biomechanical metrics of fracture healing. Additional descriptions can be found in Appendix B.

Generation of Subject Specific FE Models

Subject specific FE models were generated for 6 tibias (three each at 10 and 14 days post-fracture). After using the imaging protocol above, μCT image sets were semi-automatically segmented and boundary descriptions (as described by 3D points and 3D triangular patches) were generated through the use of a marching cubes algorithm in a commercially available image analysis software (Analyze, AnalyzeDirect) for both the entire bone/callus and just the cortical bone. Boundary descriptions of each were then used to create a heterogeneous FE tetrahedral mesh consisting of two properties (i.e. cortical bone and other material) using custom-built mesh generation methods (Sullivan et al., 1997). Once the 3D mesh is created, an image-to-grid approach is utilized which determines the voxel intensities within each tetrahedral element from the imaging domain and assigns properties based on thresholding.

Values of Poisson's ratio were assumed for all tissue types (0.3 for bone and 0.45 for callus) based on the literature (Shefelbine et al., 2005) and values associated with the near-incompressible nature of soft tissue. In addition, the cartilage and low-mineralized bone were lumped into a single isotropic property. The value of the void space elastic modulus was assumed as 0.1 Pa (many orders of magnitude below callus value). Reported values of the cortical bone modulus range from ~4 GPa to ~21 GPa (Choi et al., 1990; Jamsa et al., 1998; Schriefer et al., 2005). Because of this large variability, we

tested the inverse FEA modulus estimations to explore the impact of different cortical bone modulus values using respectively 5, 10 and 15 GPa. As reported in Appendix A, we found that the estimated callus elastic modulus did not change with the assumed cortical bone modulus (maximum of ~4.5% difference, not statistically significant). Thereafter, the 5 GPa value has been used in all the studies performed.

Simulation Studies

A cylinder mesh with three layers was created to simulate a simplified appearance of a bone fracture callus, as seen in Figure 3. The simplified geometry allows analytic comparisons to FEA results. Simulations were then performed on the cylinder mesh to test the accuracy and sensitivity of the inverse FEA procedure upon initial guess, with material properties approximating that of bone and callus (5 GPa and 1 MPa, respectively) and radius and total height of 1 mm and 6 mm, respectively. To gauge accuracy of the simulations, the forward elastic model was used to calculate boundary normal surface forces for a step displacement corresponding to 0.5% strain and compared to an analytic calculation of the surface normal force (derivation in Appendix C). The dependence of the elastographic framework on initial guess was also tested by executing simulations with five random initial callus modulus guesses.

In a separate simulation study, two meshes created from μCT imaging of a representative post-fracture day 10 and 14 tibia were used as realistic geometries for further simulation analyses. To examine the effect of mineralization compositional differences in the callus on the reconstructed lumped stiffness parameter, meshes at the two time points (representing two different phases of mineralization) were used to

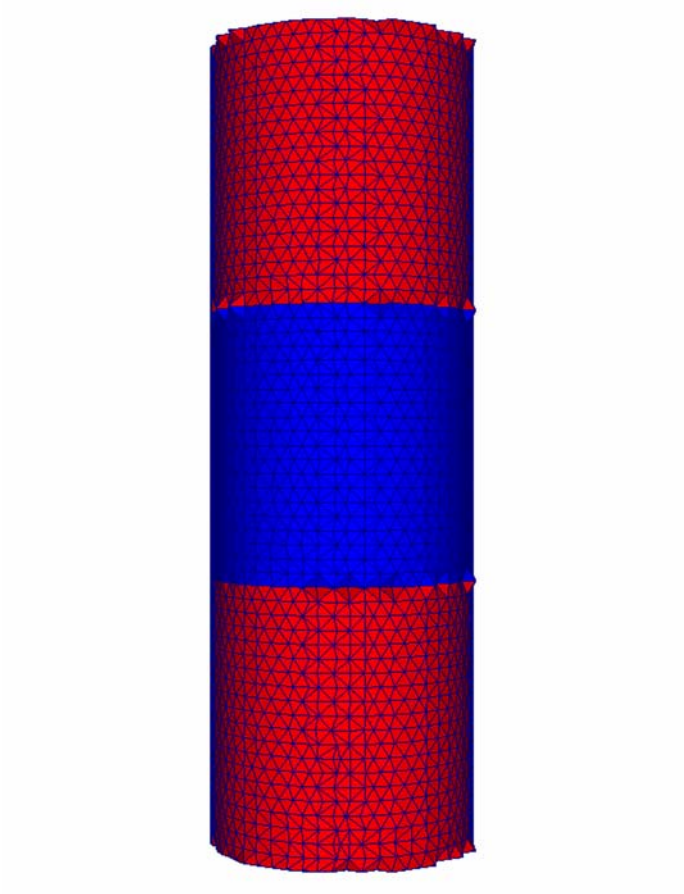

Figure 3: Cylinder mesh representing a simplified appearance of a bone fracture callus used for simulation studies. The proximal and distal layers represent the bone ends (red), while the intermediate layer represents callus (blue). Each geometrically identical layer is assumed to be a homogeneous material of dimension similar to that of a bone fracture callus.

reconstruct the combined callus stiffness. The callus material in the mesh was subdivided through thresholding into new bone and soft tissue portions and assigned separate Young's modulus values of 10 MPa and 0.1 MPa, respectively (values were arbitrarily selected to fit to actual experimental results, but are based on magnitude differences of 100 fold that have been previously suggested (Shefelbine et al., 2005)). The effect of transducer noise on the stiffness reconstruction method was also examined through the addition of Gaussian noise.

Ex Vivo Studies

Day 10 and 14 post-fracture tibias were subjected to the material property reconstruction analysis, whereby force versus displacement curves obtained from the mechanical tester were used in conjunction with the meshes generated from μCT scans to determine callus material properties. In addition, the following metrics were analyzed: (1) ultimate load, (2) toughness, (3) apparent stiffness, (3) normalized apparent stiffness, (4) total bone volume, and (5) total callus volume. More information about these metrics is reported in Appendix B.

Statistics

Data are expressed as mean ± SD. Statistical analyses were performed by comparing the analysis metrics from the independent 10 and 14 day fracture callus groups using unpaired Student's t-test, The Graph-pad Prism Software and the Power and Sample Size package software were used. Statistical significance was set at $p<0.05$; statistical power was set at 0.9

Results

Simulation 1: Validation of the FEA Model

To validate the FEA model, the simulation cylinder mesh was compared against an analytic calculation. The model was prescribed a fixed displacement of 0.5% strain and the average normal surface force was calculated from the forward FEA model as described in the Methods. The average surface normal forces were calculated as 45.0347 mN and 47.1050 mN for the model and analytic calculations, respectively, representing a 4.40 percent error in the model versus the analytic calculation, which is reasonable given the level of discretization and the type of element used (tetrahedrons tend to be slightly less accurate, but are able to more fully capture the geometry of the callus).

Simulation 2: Sensitivity of Material Property Reconstruction on Initial Guess

To determine the sensitivity of the material property reconstruction method, the forward FEA model was run as described in the Methods to generate model calculated average surface normal forces at 4 strain increments (0.5, 1.0, 1.5, and 2.0 percent strain). These results were then used as the "experimental force transducer" input along with multiple random initial guesses for the callus material property. The material property reconstruction was executed with varying initial guesses to determine the accuracy of the model to converge on the known material property given a random initial material property guess. As shown in Figure 4, the solution to the material property reconstruction converged to the correct value of 1 MPa (within 1.74 % maximum error) for all initial guesses tested.

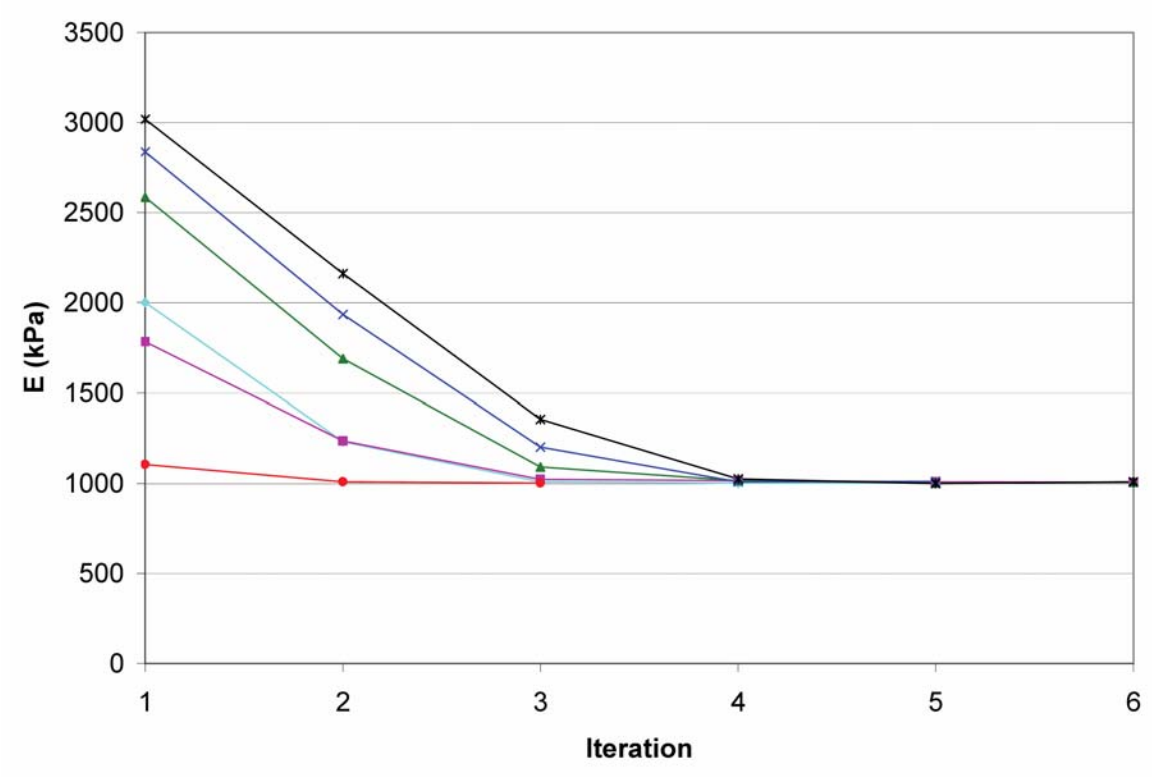

Figure 4: Convergence plot of cylinder mesh simulation with varying initial guess. The modulus (E_{callus}) converged to the optimal solution (1000 kPa) for all initial guesses tested with E_{bone} fixed at 5 GPa.

Simulation 3: Lumped Parameter Reconstruction and Sensitivity of Force Transducer Error

Representative callus meshes from 10 and 14 days post-fracture were used in simulations in which the callus was subdivided into new bone and soft tissue with modulus values as described in the Methods. The forward model was used to determine boundary normal surface forces for displacements of 0.1, 0.2, 0.3, and 0.4 mm, which were then used as the transducer force inputs to the inverse FEA with one lumped parameter corresponding to the total bulk callus modulus of elasticity. As shown in Table I, the estimated callus moduli were 1930.15 and 3538.27 kPa for the 10 and 14 day post-fracture callus meshes, respectively. These data demonstrate that changes to the new bone volume fraction (new bone/callus volume) between days 10 and 14 post-fracture result in an estimated bulk modulus of ~ 2 fold. This simulation provides some understanding of how a lumped parametric model is affected by the new bone volume fraction. The effects of transducer noise was simulated by generating noisy data sets through the addition of random Gaussian noise of 0, 1, 2, 4 and 8 standard deviations of the force transducer's listed accuracy [± 0.15 % of full scale (22 N)] to each force data point on the loading curve of the previous simulation. The noisy data sets were used to define the effects of force transducer noise on the estimated material property accuracy. As shown in Table I, the maximum error in the modulus estimation procedure was observed as 3.89% for the addition of 8 standard deviations of transducer noise (an unreasonable case and within the margin of error for the model). For the realistic scenario of 1 standard deviation of noise, the error in estimation was 9.83 kPa and 12.97 kPa, corresponding to 0.51% and 0.37% error for the 10 and 14 day calluses, respectively. This suggests that transducer noise plays little part in the overall error of the method.

Table I: Simulation results of estimated callus modulus and effects of simulated transducer noise through the addition of 0, 1, 2, 4, and 8 standard deviations of noise.

Standard deviation of noise	**$E_{model,10d}$ (kPa)**	**% error in E_{10d}**	**$E_{model,14d}$ (kPa)**	**% error in E_{14d}**
0	1930.1503	0	3538.2654	0
1	1920.3176	0.5094	3525.2906	0.3667
2	1918.8212	0.5870	3543.0592	0.1355
4	1948.7781	0.9651	3553.1002	0.4193
8	1855.0554	3.8906	3470.9360	1.9029

Material Property Estimation in Mouse Tibia Fracture Callus

Representative μCT reconstructions, corresponding meshes, and cross-sections of the meshes for both 10-day and 14-day groups are shown in Figure 5. μCT volume quantifications reported in Table II, showed a trend over an increase of callus volume and mineralization in 14 versus 10 days post-fracture. Model generated material property estimations are also compared to other biomechanical fracture healing analysis metrics (apparent stiffness, normalized apparent stiffness, and callus volume). The inverse FEA was the only test to be statistically significant in estimating a modulus that was ~4 fold increased in the 14 days post-fracture calluses compared to day 10 post-fracture (Table II). With 3 mice in each group the inverse FEA had the statistical power to detect a difference (power=0.9, alpha=0.05) between groups. These data indicate that the inverse FEA approach is sensitive to detect architectural changes that occur within the callus during the mineralization process. Although the unprocessed BMT data generated a trend of increasing stiffness for the 14 day over the 10 day post-fracture specimens, this parameter as well as all the others measured did not reach statistical significance. A large data variation was observed between samples, as clearly shown in Figure 2 that depicts the unprocessed BMT data for each sample. This large sample variation persisted following normalization of the apparent stiffness by maximal cross-sectional callus area and length (representing a conversion from apparent stiffness to elastic modulus), indicating the inadequacy of volumetric normalization.

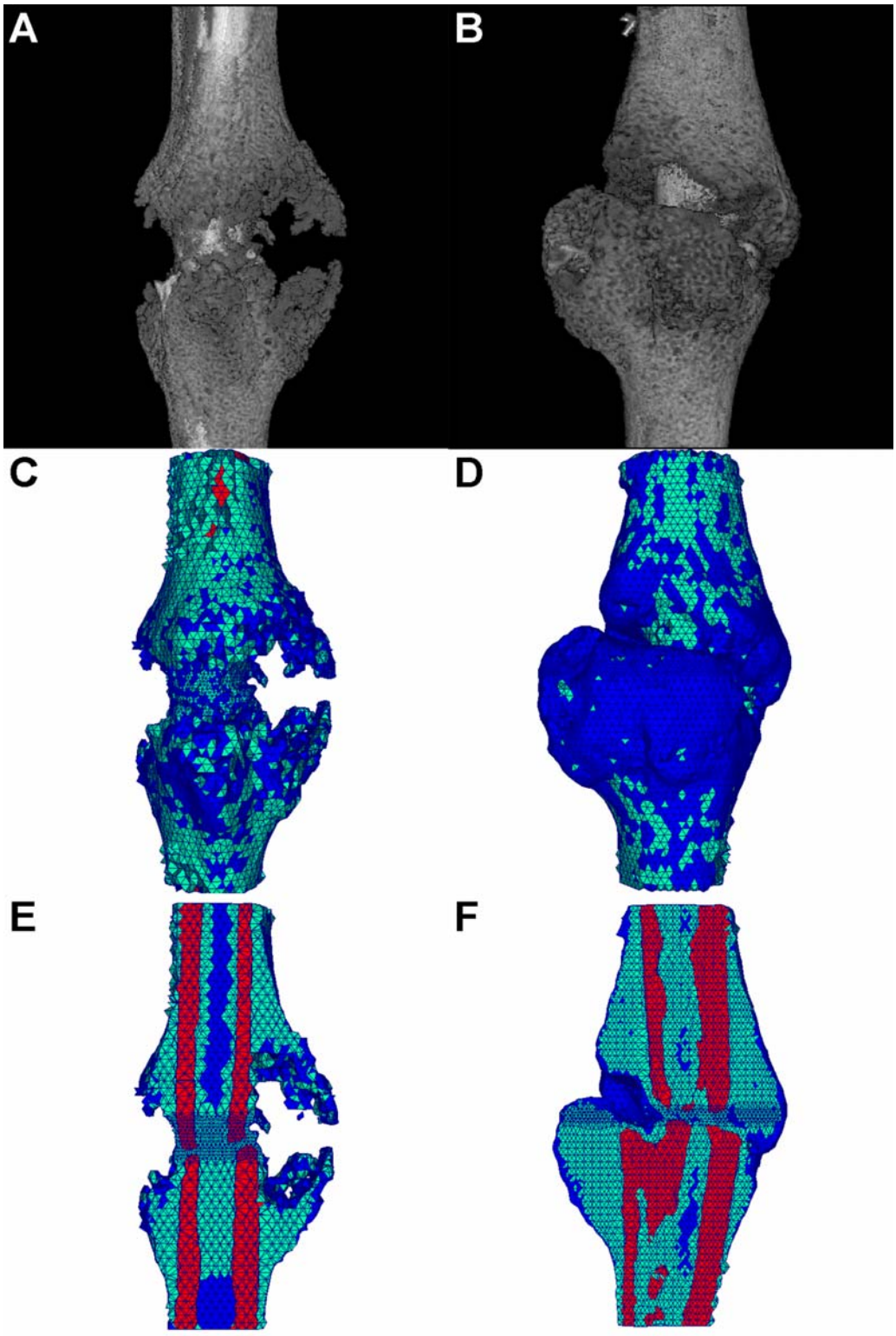

Figure 5: (A,B) Representative μCT 3-D reconstructions for mouse tibia fracture, (C,D) corresponding tetrahedral FE meshes, (E,F) cut-away images of the tetrahedral FE meshes showing internal elements and material types. Element colors represent material type of bone (red), callus (green), and void (blue). (A,C,E) 10 day post-fracture, (B,D,F) 14 day post-fracture.

Table II: Comparison of BMT and CT fracture healing analysis metrics with estimated callus elastic modulus for 10 and 14 days post-fracture samples. Numbers are expressed as mean +/- SD and P values are reported using unpaired Student's t-test. * denotes statistically significant difference.

	10 d (n=3)	**14 d (n=3)**	**P Value**
Ultimate Load (N)	1.560 ± 0.1370	1.643 ± 0.4888	0.7902
Toughness (N*mm)	0.4059 ± 0.08796	0.1957 ± 0.1567	0.1127
Apparent Stiffness (N/mm)	4.744 ± 2.345	13.95 ± 6.241	0.0751
Normalized Apparent Stiffness (kPa)	3885 ± 1800	8330 ± 4941	0.2170
Total Bone Volume (new bone + cortical bone) (mm^3)	4.051 ± 0.1183	5.894 ± 1.355	0.0788
Total Callus Volume (soft tissue + new bone) (mm^3)	4.391 ± 1.051	8.772 ± 3.772	0.1257
$E_{estimated}$ (kPa)	797.1 ± 414.3	2908 ± 872.8	0.0194 *

Discussion

In this study we have developed an inverse FEA procedure to determine the elastic modulus in mouse tibia fracture callus based on μCT/histological threshold data and data acquired from tensile BMT analyses. The FEA showed: 1) less than 5% error compared to the analytic calculations; 2) a sensitivity of material property estimation within 1.74% maximal error for measurement error as large as 8 SD; 3) appropriate sensitivity in estimating the modulus changes expected during two distinct time points of the fracture healing process.

The healing length of the stabilized mouse tibia fracture model is ~28 days (Hiltunen et al., 1993). We have performed our studies at post-fracture days 10 and 14. As assessed by histological analyses in this time window the callus is in its most active healing phase and has not yet reached the remodeling phase (Hiltunen et al., 1993). It is reasonable to assume that the mechanical properties of the callus should become progressively better and more functionally stable over time. As a result, metrics focused at assessing healing should improve between these time points. BMT has been considered the gold-standard technique to assess the mechanical properties of the callus and therefore the healing progression. However, in our studies we found that BMT was not sensitive enough to detect significant differences in any of thee metrics between the time points studied. It is likely that the mechanical improvement has been masked by confounding geometrical factors that determined a wide data variation, even after maximal cross-sectional area and callus length normalizations. These BMT data, left alone, would have led to the paradoxical conclusion that a rapid healing progression would not be reflected by an improvement in mechanical stability. This lack of BMT

sensitivity clearly highlights the need for alternative methods to detect material property changes during the healing process. Due to the large variance of the apparent stiffness measurements, it is possible that the inability of this method to detect a difference may be due to the small sample size. We estimated that 6 mice for each group would have been needed to get a statistical power of 0.9. On the other hand, using equal power analysis, only 3 mice for each group were needed to detect a difference between groups using the inverse FEA model. This indicates that because of the small variance, our model is powerful in detecting subtle differences in material properties therefore reducing the usage of mice, experimental time and expenses.

Through simulation studies, the inverse FEA approach developed in this work is shown to accurately calculate surface normal forces and to converge on a preset modulus value using random initial guess in the presence of transducer noise. Through ex vivo specimen analysis, the approach was able to detect a difference in the callus material modulus of ~4 fold from post-fracture day 10 to day 14. Taken together with the simulation analysis of callus meshes with both new bone and cartilaginous tissue material components, these data suggest that between 10 and 14 days post-fracture, there is a significant change in material composition (new bone volume fraction) that results in stiffness increase. In future studies, the inverse FEA approach will allow for establishing the temporal pattern of material property changes throughout the entire course of the healing process in normal and genetically/therapeutically manipulated fracture calluses.

In our model we have only incorporated the linear component of the force/displacement curves, but fracture healing can also be characterized by both geometrical and material nonlinearities. We recognize that our model, in lacking the

nonlinear component, has some limitations. However, as depicted in Figure 2 the linear component accounts for 75 ± 24.2% of the curve(s) indicating that a significant amount of the callus follows a linear modality in force/displacement testing. We acknowledge that this analysis only begins to address the question of constitutive modeling, but, it is important in that it demonstrates that first order approximations of subject specific models offer discriminatory power regarding fracture healing state analysis. The discriminatory power produced by the model created within this work can allow for more accurate functional mechanical analysis of fracture calluses that: (1) establish normative data regarding the longitudinal change in normal fracture callus properties, (2) aid in the analysis of therapeutic treatment options for improvement/acceleration of fracture healing, and (3) assist in earlier and more effective clinical determination of fracture non-union.

CHAPTER III

FUTURE WORK

The current work has shown significant relevance and improved analysis of the inverse FEA method for differential analysis between mechanical properties of fracture calluses from two time points of normal fracture healing in normal mice. However, analysis of normal fractures in normal mice helps only to characterize the progression of mechanical properties during unimpeded fracture healing. The goal of fracture healing studies remains: (1) diagnosis of pathological fracture healing failure and evaluation of pathological fracture non-unions; and (2) evaluation of experimental therapeutic methods that aim to enhance the normal and/or pathological fracture healing process. Therefore the goal of future work is to test/validate the analysis method against experimental pathological and therapeutic models. Pathological and/or therapeutic fracture healing models prove challenging for regular BMT analysis due to vast differences in callus geometry and architecture, making current beam-theory based mechanical analysis especially prone to significant error. However with the incorporation of both BMT and μCT data in the current analysis, we hypothesize that the inverse FEA method will generate more accurate and sensitive mechanical assessment of treatment efficacy or pathological diagnosis.

The FEA modeling procedure described within this work showed reconstructed values that were consistent among the widely distributed force/displacement curves. It is interesting to note that the modeling analysis was the only metric to show statistical

significance among other commonly used healing assessment metrics. This suggests that model-based inverse analysis produces a more consistent metric. However, the procedure still has shortcomings at this early stage. These shortcomings are mainly related to certain assumptions used to define the model, and include: (1) the choice of tetrahedral elements versus hexahedral elements, which tend to more accurately reflect mechanics modeling, (2) the high strain conditions within the fracture gap likely need the full-nonlinear strain tensor description instead of small strain theory, and (3) the assumptions of Hookean elasticity. It is the goal of future studies to address these shortcomings with more refined FEA.

APPENDIX

Appendix A: Supplemental Table I: Comparison of estimated callus elastic modulus for 10 and 14 days post fracture samples with differing values for cortical bone elastic modulus. Numbers are expressed as mean +/- SD and P values are reported using unpaired Student's t-test. ***** denotes statistically significant difference between 10 and 14 day groups.

	10 d (n=3)	**14 d (n=3)**	**P Value**
$E_{estimated}$ (kPa) w/ $E_{cortical}$ = 5 GPa	797.1094 ± 414.295	2908.294 ± 872.809	0.0194 *
$E_{estimated}$ (kPa) w/ $E_{cortical}$ = 10 GPa	762.4152 ± 404.8187	2813.223 ± 825.9909	0.0181 *
$E_{estimated}$ (kPa) w/ $E_{cortical}$ = 15 GPa	769.7466 ± 385.6674	2788.968 ± 786.6818	0.0162 *

Appendix B: Additional descriptions of methods

Inverse Problem Framework

To determine the callus modulus, the model calculated average force (F_{calc}) is generated from an initial callus Young's modulus guess (E). A custom-built Levenberg-Marquardt non-linear optimization algorithm is used to iteratively optimize the modulus value such that F_{calc} approaches the experimental material tester generated force (F_{exptl}). In this approach, each strain level is treated as an independent data point with respect to determining the modulus. This allows the formation of an objective function from the elastic portion of the force-displacement data, i.e.

$$G(E) = \sum_{i=1}^{N} \left(F_{calc} - F_{exp\,tl}\right)_i^2$$

where N is the number of data points along the elastic region of the force-displacement curve. In this case, we are solving for a single property which represents the elastic modulus (E) of the 'lumped' callus region. To optimize this for the callus modulus, we take the derivative of our objective function, G(E) and set equal to zero.

$$\frac{dG(E)}{dE} = \left[\frac{\partial F_{calc\,1}}{\partial E} \quad \frac{\partial F_{calc\,2}}{\partial E} \quad \cdots \quad \frac{\partial F_{calcN}}{\partial E}\right] \begin{Bmatrix} F_{calc\,1} - F_{exp\,tl1} \\ F_{calc\,2} - F_{exp\,tl2} \\ \vdots \\ F_{calcN} - F_{exp\,tlN} \end{Bmatrix} = 0$$

or simplified as,

$$[J]^T \left\{\overline{F}_{calc} - \overline{F}_{exp\,tl}\right\} = 0 .$$

From this, a standard Levenberg-Marquardt framework can be used to solve this root problem,

$$\left([J]^T[J] + \alpha I\right)\Delta E = [J]^T\left\{\overline{F}_{calc} - \overline{F}_{exp\ tl}\right\}$$

where ΔE is the change in material property for the iterative method, i.e.

$$E_{i+1} = E_i + \Delta E,$$

and α is a regularization term to improve the conditioning of the iterative procedure and is defined as,

$$\alpha = \left(\lambda * \text{trace}\left([J]^T[J]\right) * SSE^2\right)^{1/2}$$ (Joachimowicz et al., 1991)

where λ is an empirical factor, and SSE is the sum squared error between measured and calculated force. It should be noted that the Jacobian was determined by a finite difference calculation which was initiated by a 2.5% perturbation from the initial guess of the callus property. As schematically presented in Figure 1, the process is repeated until the relative error between iterations converges below a set tolerance or until no improvement in objective function is noted and a unique solution is found.

Material Type Description Based on μCT/Histological Thresholding Analysis

To determine material type from μCT scans, a parametric thresholding study was performed by serial μCT scanning and histological analysis. Fractured tibia calluses were dissected, fixation pins removed, and μCT scanned at 6 μm voxel resolution. Bones were then fixed for 48 h at 4 °C in 4% paraformaldehyde solution, and decalcified for 10 days in an EDTA decalcification solution (10 mM Tris-HCl, 10% EDTA, 7.5% polyvinylpirrolidone pH 7.5). Bones were dehydrated in a graded ethanol series, embedded in paraffin, and sectioned at 6 μm thickness along ~5.2 mm length centered at the fracture line. This resulted in 864 histological sections per bone, which were placed 3 sections per slide and divided into 4 serial groups for staining, resulting in ~72 slides per

group (72 slides x 3 sections/slide x 4 groups). *In-situ* hybridizations for Collagen 1 and Collagen 10 and Trichrome Blue and Safranin O/Fast Green histological staining were performed to identify tissue type. Trichrome Blue and Safranin O/Fast Green staining were obtained using standard histological procedures as previously described (Jingushi et al., 1992). Collagen 1 *in situ* hybridization was used to label new bone, Collagen 10 *in situ* hybridization to label hypertrophic chondrocytes; Safranin O/Fast Green staining to label areas of cartilaginous tissue as bright red and areas of bone as green; Trichrome Blue staining to label newly mineralized bone as blue and highly mineralized bone as red. *In situ* hybridization analysis was performed as previously reported (Spagnoli et al., 2007). Plasmid with insertion of mouse Collagen (I)-alpha-1-chain (Col1a1) by G. Karsenty (Columbia University). Probe for mouse Collagen (X)alpha1chain (Col10a1) was generated as previously described (Spagnoli et al., 2007). Each histological marker was quantified by a custom built image analysis code written in MATLAB (Mathworks Inc., Natick, MA) that was used to select tissue type (cartilage tissue, new bone, and cortical bone) based on color intensity. Groups were quantified by summation of voxels and multiplied by voxel volume to yield volume of tissue. The μCT image stack was then thresholded based on radiodensity into the 3 groups that visually and quantitatively matched histological staining determination of tissue type. The soft tissue and new bone regions were lumped together and defined as callus material and the cortical bone regions were taken to be cortical bone material.

Description of analysis metrics

BMT metrics:

Ultimate load is defined as the peak force recorded during the BMT procedure. Toughness is defined as the area under the Force vs. displacement curve from the origin to the point of ultimate load. Apparent stiffness is defined as the slope of a best fit line to the linear portion of the force versus displacement curve during the loading phase. Normalized apparent stiffness is defined as apparent stiffness with the force and displacement values normalized by dividing by the largest cross-sectional area of the callus and its overall length, respectively.

Imaging metrics:

Total bone volume was determined by summing the voxels corresponding to mineralized tissue (new bone and cortical bone), then multiplying by the voxel resolution. Total callus volume was determined by summing the voxels corresponding to callus tissue (soft tissue and new bone), then multiplying by the voxel resolution.

Appendix C: Derivation of simulation force: The analytic derivation of the surface normal force for a three part cylinder (represented in Figure 3) is shown.

We start with Hooke's law, where stress, strain, and Young's modulus are represented by σ, ε, and E, respectively.

$$\sigma = E\varepsilon \tag{1}$$

Then we substitute the definitions for stress and strain, where P, A, δ, and L represent respectively force, cross-sectional area, displacement, and length.

$$\frac{P}{A} = E\frac{\delta}{L} \tag{2}$$

Solving (2) for displacement yields:

$$\delta = \frac{PL}{EA} \tag{3}$$

We then take note that the total displacement is equal to the sum of the displacements in each section of the cylinder.

$$\delta = \delta_1 + \delta_2 + \delta_3 \tag{4}$$

We also take note that the total force is equal throughout the total cylinder.

$$P = P_1 = P_2 = P_3 \tag{5}$$

Substitute (3) into (4).

$$\delta = \frac{P_1 L_1}{E_1 A_1} + \frac{P_2 L_2}{E_2 A_2} + \frac{P_3 L_3}{E_3 A_3} \tag{6}$$

Because each portion of the cylinder is of equal length and cross-sectional area ($L = L_1 = L_2 = L_3$ and $A = A_1 = A_2 = A_3$) and from (5), (6) can be written as,

$$\delta = \frac{PL}{A}\left(\frac{1}{E_1} + \frac{1}{E_2} + \frac{1}{E_3}\right) \tag{7}$$

Since E1 = E3 (both cylinder sections represent bone), the force can be written as:

$$P = \frac{\delta A}{L}\left(\frac{E_1 E_2}{2E_2 + E_1}\right) \tag{8}$$

REFERENCES

Barnes, S. L., Lyshchik, A., Washington, M. K., Gore, J. C., Miga, M. I., 2007. Development of a mechanical testing assay for fibrotic murine liver. Medical Physics 34(11), 4439-4450.

Bourne, B. C., van der Meulen, M. C., 2004. Finite element models predict cancellous apparent modulus when tissue modulus is scaled from specimen CT-attenuation. J Biomech 37(5), 613-21.

Capdevila, J., Izpisua Belmonte, J. C., 2001. Patterning mechanisms controlling vertebrate limb development. Annu Rev Cell Dev Biol 17, 87-132.

Cattermole, H. C., Fordham, J. N., Muckle, D. S., Cunningham, J. L., 1996. Dual-energy x-ray absorptiometry as a measure of healing in fractures treated by intramedullary nailing. Journal of Orthopaedic Trauma 10(8), 563-568.

Chen, Y., Zhao, X., 1998. Shaping limbs by apoptosis. J Exp Zool 282(6), 691-702.

Choi, K., Kuhn, J. L., Ciarelli, M. J., Goldstein, S. A., 1990. The elastic moduli of human subchondral, trabecular, and cortical bone tissue and the size-dependency of cortical bone modulus. J Biomech 23(11), 1103-13.

Ciprian, S., Iochum, S., Kohlmann, R., Dautel, G., Dap, F., Blum, A., 2004. MR imaging accuracy in the prediction of bone graft healing potential in scaphoid non-union. Journal De Radiologie 85(10), 1699-1706.

Colnot, C., Thompson, Z., Miclau, T., Werb, Z., Helms, J. A., 2003. Altered fracture repair in the absence of MMP9. Development 130(17), 4123-4133.

Einhorn, T. A., 1995. Enhancement of fracture-healing. J Bone Joint Surg Am 77(6), 940-56.

Einhorn, T. A., 1998. The cell and molecular biology of fracture healing. Clinical Orthopaedics and Related Research(355), S7-S21.

Ganan, Y., Macias, D., Duterque-Coquillaud, M., Ros, M. A., Hurle, J. M., 1996. Role of TGF beta s and BMPs as signals controlling the position of the digits and the areas of interdigital cell death in the developing chick limb autopod. Development 122(8), 2349-57.

Gerstenfeld, L. C., Wronski, T. J., Hollinger, J. O., Einhorn, T. A., 2005. Application of histomorphometric methods to the study of bone repair. Journal of Bone and Mineral Research 20(10), 1715-1722.

Granero-Molto, F., Weis, J. A., Longobardi, L., Spagnoli, A., 2008. Role of mesenchymal stem cells in regenerative medicine: application to bone and cartilage repair. Expert Opin Biol Ther 8(3), 255-68.

Granero-Molto, F., Weis, J. A., O'Rear, L. D., Miga, M. I., Spagnoli, A., 2007. IGF-I engineered bone marrow mesenchymal stem cells improve the fracture healing process. Journal of Bone and Mineral Research 22, S105-S105.

Greenleaf, J. F., Fatemi, M., Insana, M., 2003. Selected methods for imaging elastic properties of biological tissues. Annual Review of Biomedical Engineering 5, 57-78.

Grigoryan, M., Lynch, J. A., Fierlinger, A. L., Guermazi, A., Fan, B., MacLean, D. B., MacLean, A., Genant, H. K., 2003. Quantitative and qualitative assessment of closed fracture healing using computed tomography and conventional radiography. Academic Radiology 10(11), 1267-1273.

Gutierrez, G. E., Edwards, J. R., Jarrett, I. R., Nyman, J. S., Mccluskey, B., Rossini, G., Flores, A., Neidre, D. B., Mundy, G. R., 2008. Transdermal Lovastatin Enhances Fracture Repair in Rats. Journal of Bone and Mineral Research 23(11), 1722-1730.

Hall, B. K., Miyake, T., 1992. The membranous skeleton: the role of cell condensations in vertebrate skeletogenesis. Anat Embryol (Berl) 186(2), 107-24.

Hall, B. K., Miyake, T., 1995. Divide, accumulate, differentiate: cell condensation in skeletal development revisited. Int J Dev Biol 39(6), 881-93.

Hall, B. K., Miyake, T., 2000. All for one and one for all: condensations and the initiation of skeletal development. Bioessays 22(2), 138-47.

Hiltunen, A., Vuorio, E., Aro, H. T., 1993. A Standardized Experimental Fracture in the Mouse Tibia. Journal of Orthopaedic Research 11(2), 305-312.

Holzer, G., Majeska, R. J., Lundy, M. W., Hartke, J. R., Einhorn, T. A., 1999. Parathyroid hormone enhances fracture healing - A preliminary report. Clinical Orthopaedics and Related Research(366), 258-263.

Hsu, W. K., Feeley, B. T., Krenek, L., Stout, D. B., Chatziioannou, A. F., Lieberman, J. R., 2007. The use of F-18-fluoride and F-18-FDG PET scans to assess fracture healing in a rat femur model. European Journal of Nuclear Medicine and Molecular Imaging 34(8), 1291-1301.

Huddleston, P. M., Steckelberg, J. M., Hanssen, A. D., Rouse, M. S., Bolander, M. E., Patel, R., 2000. Ciprofloxacin inhibition of experimental fracture-healing. Journal of Bone and Joint Surgery-American Volume 82A(2), 161-173.

Jamsa, T., Jalovaara, P., Peng, Z., Vaananen, H. K., Tuukkanen, J., 1998. Comparison of three-point bending test and peripheral quantitative computed tomography analysis in the evaluation of the strength of mouse femur and tibia. Bone 23(2), 155-161.

Jingushi, S., Joyce, M. E., Bolander, M. E., 1992. Genetic expression of extracellular matrix proteins correlates with histologic changes during fracture repair. J Bone Miner Res 7(9), 1045-55.

Joachimowicz, N., Pichot, C., Hugonin, J. P., 1991. Inverse Scattering - an Iterative Numerical-Method for Electromagnetic Imaging. Ieee Transactions on Antennas and Propagation 39(12), 1742-1752.

Lynch, J. A., Grigoryan, M., Fierlinger, A., Guermazi, A., Zaim, S., MacLean, D. B., Genant, H. K., 2004. Measurement of changes in trabecular bone at fracture sites using X-ray CT and automated image registration and processing. Journal of Orthopaedic Research 22(2), 362-367.

Macias, D., Ganan, Y., Rodriguez-Leon, J., Merino, R., Hurle, J. M., 1999. Regulation by members of the transforming growth factor beta superfamily of the digital and interdigital fates of the autopodial limb mesoderm. Cell Tissue Res 296(1), 95-102.

Mariani, F. V., Martin, G. R., 2003. Deciphering skeletal patterning: clues from the limb. Nature 423(6937), 319-25.

Marsh, D., 1998. Concepts of fracture union, delayed union, and nonunion. Clinical Orthopaedics and Related Research(355), S22-S30.

Miga, M. I., Rothney, M. P., Ou, J. J., 2005. Modality independent elastography (MIE): Potential applications in dermoscopy. Medical Physics 32(5), 1308-1320.

Ophir, J., Cespedes, I., Ponnekanti, H., Yazdi, Y., Li, X., 1991. Elastography - a Quantitative Method for Imaging the Elasticity of Biological Tissues. Ultrasonic Imaging 13(2), 111-134.

Ou, J. J., Ong, R. E., Yankeelov, T. E., Miga, M. I., 2008. Evaluation of 3D modality-independent elastography for breast imaging: a simulation study. Physics in Medicine and Biology 53(1), 147-163.

Reynolds, D. G., Hock, C., Shaikh, S., Jacobson, J., Zhang, X., Rubery, P. T., Beck, C. A., O'Keefe R, J., Lerner, A. L., Schwarz, E. M., Awad, H. A., 2007. Micro-computed tomography prediction of biomechanical strength in murine structural bone grafts. J Biomech 40(14), 3178-86.

Roark, E. F., Greer, K., 1994. Transforming growth factor-beta and bone morphogenetic protein-2 act by distinct mechanisms to promote chick limb cartilage differentiation in vitro. Dev Dyn 200(2), 103-16.

Samani, A., Plewes, D., 2007. An inverse problem solution for measuring the elastic modulus of intact ex vivo breast tissue tumours. Physics in Medicine and Biology 52(5), 1247-1260.

Saran, N., Hamdy, R. C., 2008. DEXA as a Predictor of Fixator Removal in Distraction Osteogenesis. Clinical Orthopaedics and Related Research 466(12), 2955-2961.

Schmidhammer, R., Zandieh, S., Mittermayr, R., Pelinka, L. E., Leixnering, M., Hopf, R., Kroepfl, A., Redl, H., 2006. Assessment of bone union/nonunion in an experimental model using microcomputed technology. Journal of Trauma-Injury Infection and Critical Care 61(1), 199-205.

Schriefer, J. L., Robling, A. G., Warden, S. J., Fournier, A. J., Mason, J. J., Turner, C. H., 2005. A comparison of mechanical properties derived from multiple skeletal sites in mice. Journal of Biomechanics 38(3), 467-475.

Severns, A. E., Lee, Y. P., Nelson, S. D., Johnson, E. E., Kabo, J. M., 2004. Metabolic measurement techniques to assess bone fracture healing - A preliminary study. Clinical Orthopaedics and Related Research(424), 231-238.

Shefelbine, S. J., Simon, U., Claes, L., Gold, A., Gabet, Y., Bab, I., Muller, R., Augat, P., 2005. Prediction of fracture callus mechanical properties using micro-CT images and voxel-based finite element analysis. Bone 36(3), 480-8.

Spagnoli, A., O'Rear, L., Chandler, R. L., Granero-Molto, F., Mortlock, D. P., Gorska, A. E., Weis, J. A., Longobardi, L., Chytil, A., Shimer, K., Moses, H. L., 2007. TGF-beta signaling is essential for joint morphogenesis. J Cell Biol 177(6), 1105-17.

Sullivan, J. M., Charron, G., Paulsen, K. D., 1997. A three-dimensional mesh generator for arbitrary multiple material domains. Finite Elements in Analysis and Design 25(3-4), 219-241.

van Lenthe, G. H., Voide, R., Boyd, S. K., Muller, R., 2008. Tissue modulus calculated from beam theory is biased by bone size and geometry: implications for the use of three-point bending tests to determine bone tissue modulus. Bone 43(4), 717-23.

Washington, C. W., Miga, M. I., 2004. Modality independent elastography (MIE): A new approach to elasticity imaging. Ieee Transactions on Medical Imaging 23(9), 1117-1128.

Zachos, T., Diggs, A., Weisbrode, S., Bartlett, J., Bertone, A., 2007. Mesenchymal stem cell-mediated gene delivery of bone morphogenetic protein-2 in an articular fracture model. Molecular Therapy 15(8), 1543-1550.

Zhao, M., Zhao, Z., Koh, J. T., Jin, T. C., Franceschi, R. T., 2005. Combinatorial gene therapy for bone regeneration: Cooperative interactions between adenovirus vectors expressing bone morphogenetic proteins 2, 4, and 7. Journal of Cellular Biochemistry 95(1), 1-16.